IEEE Access
Multidisciplinary | Rapid Review | Open Access Journal

Received February 16, 2021, accepted February 25, 2021, date of publication March 2, 2021, date of current version March 10, 2021.

Digital Object Identifier 10.1109/ACCESS.2021.3063461

Detection of Malfunctioning Photovoltaic Modules Based on Machine Learning Algorithms

HUMBLE PO-CHING HWANG[1,2], COOPER CHENG-YUAN KU[1], (Member, IEEE), AND JAMES CHI-CHANG CHAN[2]

[1]Institute of Information Management, National Yang Ming Chiao Tung University, Hsinchu 30010, Taiwan
[2]Industrial Technology Research Institute (ITRI), Hsinchu 31040, Taiwan

Corresponding author: Cooper Cheng-Yuan Ku (cooperku@nycu.edu.tw)

This work was supported in part by the Ministry of Science and Technology in Taiwan under Grant MOST 106-2410-H-009-025-MY3, and in part by the Industrial Technology Research Institute in Hsinchu under Grant 107C411 and Grant 108A406.

ABSTRACT In recent years, with the rise of environmental awareness worldwide, the number of solar power plants has significantly increased. However, the maintenance of solar power plants is not an easy job, especially the detection of malfunctioning photovoltaic (PV) cells in large-scale or remote power plants. Therefore, finding these cells and replacing them in time before severe events occur is increasingly important. In this paper, we propose a hybrid scheme with three embedded learning methods to enhance the detection of malfunctioning PV modules with validated efficiencies. For the first method, we combine the improved gamma correction function (preprocess) with a convolutional neural network (CNN). Infrared (IR) thermographic images of solar modules are used to train the abovementioned improved algorithm. For the second method, we train a CNN model using the IR temperatures of PV modules with the preprocessing of a threshold function. A compression procedure is then designed to cut the time-consuming preprocesses. The third method is to replace the CNN with the eXtreme Gradient Boosting (XGBoost) algorithm and the selected temperature statistics. The experimental results show that all three methods can be implemented with high detection accuracy and low time consumption, and furthermore, the hybrid scheme provides an even better accuracy.

INDEX TERMS Solar power generation, fault detection, infrared imaging, image processing, machine learning.

I. INTRODUCTION

Recently, renewable energy sources (RESs), such as wave power, wind power, and solar energy, have undergone impressively fast evolution. In Taiwan, the solar industry is specifically playing a critical role in the clean and low-carbon energy industry due to climatic factors; therefore, the quantity of solar power plants has grown rapidly. In addition to many factories, many families install PV modules on the roofs of houses, buildings, yards, etc. However, solar modules may suffer from malfunctions such as open circuits, cracks, bird droppings or heavy dust from time to time. Hence, the maintenance of solar modules is crucially important to avoid safety events, especially for very large solar power plants or remote plants. The traditional method involves maintenance personnel patrolling the whole plant to take IR images for the detection of malfunctioning PV modules. This measure can be used to detect different kinds of malfunctions, and it is nondestructive, contactless and efficient. Actually, in both [1] and [2], authors have proven that infrared thermography is able to detect all kinds of malfunctioning PV modules. There are three major types of malfunctioning PV modules, i.e., hot spots, potential-induced degradation (PID) and open circuits. They are summarized as follows, and the corresponding IR images are illustrated in Fig. 1.

1) Hot spot: A hot spot is the most common PV module defect. A hot spot results in a higher temperature and may be caused by many reasons, including short circuits, overhead objects, surface fouling, cell material defects, cell cracks, broken glass, and so on.
2) PID: PID is a condition that may occur a few years after installation. It can be caused by humidity, heat or voltage. The temperature of the malfunctioned cell

The associate editor coordinating the review of this manuscript and approving it for publication was Xiaodong Liang.

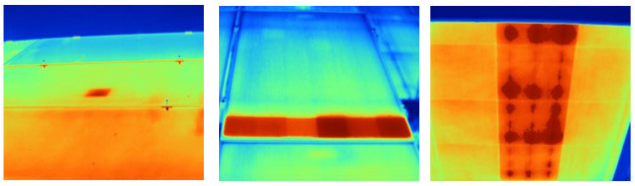

(a) (b) (c)

FIGURE 1. IR images of different PV module malfunctions, (a) hot spot, (b) PID, and (c) open circuit.

is also higher than others and results in a larger and extremely hot area.

3) Open circuit: An open circuit of a PV module causes a higher temperature in this array than other arrays. Therefore, as shown in the IR image of Fig. 1(c), the temperature of an open-circuit module array is extraordinarily red.

However, the detection of malfunctioning solar modules is not effortless because it takes large amounts of time and human labor, especially for very large or remote solar plants. With the advancement of technology, some detection teams use unmanned aerial vehicles (UAVs) equipped with infrared cameras to search for malfunctioning PV modules. In addition to a wide working range, drones may also patrol some unreachable locations. Therefore, in this paper, we design a hybrid scheme with three procedures that use an infrared camera on a UAV to take IR images and then analyze them using machine/deep learning algorithms to detect malfunctioning PV modules or classify malfunction types. In the first procedure, the enhanced infrared images of solar panels are used to train the deep learning model to automatically identify malfunctions. In the second one, the adjusted temperatures of all pixels of the IR image are used to train the deep learning model. For the third one, the characteristics of temperatures are used for training the machine learning model. The experimental results validate that all three methods can save labor and time when detecting malfunctioning modules. Furthermore, a hybrid scheme adopting the above three methods shows even better performance.

The contributions of this study are briefly summarized as follows. (I) We improve the ''gamma correction'' image processing algorithm that is used to enhance the contrast between normal and abnormal cells and then build the CNN-based procedure to detect PV module defects. (II) To stress the contrast of malfunctioning locations for the temperature dataset, we also design a threshold function to preprocess the temperatures. (III) To the best of our knowledge, our proposals are the first to adopt temperature data for training. (IV) Our model can also differentiate PIDs, open circuits and hot spots well. (V) A hybrid detection scheme with even better performance is proposed.

II. RELATED TECHNIQUES AND WORKS

A. MACHINE LEARNING AND DEEP LEARNING

With the advancement of information technology, artificial intelligence (AI) has become the most important research and application topic. Many fields need AI to intelligently save time and human labor costs. Machine learning, a branch of AI, is a type of smart method that learns from data, identifies patterns and makes decisions with less human intervention. Machine learning is applied in many fields, such as finance, image recognition, object detection, weather, and medical research. Recently, deep learning, which is a subset of machine learning that includes networks capable of conducting unsupervised learning from unstructured or unlabeled data, has boomed. Many deep learning algorithms have been proven to be very powerful, such as CNNs, recurrent neural networks (RNNs), and long short-term memory (LSTM). Among them, the CNN has been widely used in the field of image processing because it is especially good at image classification and recognition.

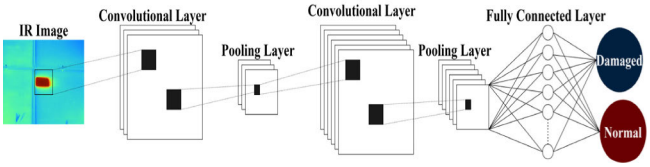

FIGURE 2. Illustration of the CNN architecture.

The CNN is a backpropagation algorithm built by modeling brain functions. This network employs a mathematical operation named the convolution, which is a specialized kind of linear operation. The CNN extracts the feature boundaries of the object and learns to perform recognition through a series of layered operations. The architecture of the CNN is composed of multiple convolutional layers, pooling layers, rectified linear unit (ReLU) layers, loss layers and fully connected layers, as shown in Fig. 2.

In [3], the authors trained a CNN model to classify 1.2 million images into 1000 different classes in the ImageNet LSVRC 2010 contest. A customized CNN was also used to classify lung image patches with interstitial lung disease [4]. The results of both [3] and [4] demonstrate that the CNN is suitable for image recognition and classification.

XGBoost, a well-known machine learning technique, is an improved version of the gradient boosting decision tree (GBDT) [5]. XGBoost combines the gradient boosting and gradient descent algorithms and is primarily adopted for supervised learning. The different features of XGBoost and GBDT include the clever penalization of trees, a proportional shrinking of leaf nodes, an extra randomization parameter and Newton boosting [6]. The objective function of XGBoost is composed of two parts, as indicated in (1) [5]. The first term, $\sum_i l\left(\hat{y}_i, y_i\right)$, is the training loss of the model and measures the difference between the predicted value and the target value. The second term, $\sum_k \Omega\left(f_k\right)$, is a normalization part in which the penalty is generated to control the complexity (the number of leaves) of the model, and the score weight of each leaf node is added to prevent overfitting [5].

$$obj\left(\phi\right) = \sum\nolimits_i l\left(\hat{y}_i, y_i\right) + \sum\nolimits_k \Omega\left(f_k\right) \tag{1}$$

where $\Omega\left(f\right) = \gamma T + \frac{1}{2}\lambda \left\|w\right\|^2$.

Another major difference between XGBoost and GBDT is that it uses the Taylor series in the objective function, which makes the convergence of XGBoost faster than that of GBDT. XGBoost is widely used by data scientists to solve many machine learning problems in practice [7]–[8].

B. IMAGE PREPROCESSING

1) GAMMA CORRECTION FUNCTION

The gamma correction function is often used to correct an image's luminance [9]. This function is defined by the following power-law expression:

$$V_{out} = aV_{in}^{\gamma} \tag{2}$$

where V_{in} is the input value, V_{out} is the output value, a is a constant and γ is the power. To make the difference between the abnormal and normal locations of IR images more obvious, we design an improved gamma correction function to achieve better preprocessing performance.

2) OTHER IMAGE PROCESSING TECHNIQUES

Some image-processing techniques, such as Canny edge detection and Gaussian filtering, have also been proposed to enhance the detection of malfunctioning PV modules. In [10], the authors used a Gaussian filter and a binary model to determine the defect and degradation percentages of PV modules. In [11], both the thermal image process and Canny edge detection technique were used to detect the module-related faults that lead to hot-spot malfunctions.

C. LITERATURE REVIEW

There have been some published methods for detecting damaged PV modules. Chouder and Silvestre presented a method based on power-loss data analysis to automatically detect faults in a PV system [12]. To calculate the main parameters of the PV system from monitoring data, a parameter extraction method was adopted. In [13], the authors proposed a deep learning-based method to detect and classify the defects of PV modules. The CNN was used to extract features from 2-D scalograms of system data. This approach could effectively classify five different faulty cases. Another type of fault detection method was based on electroluminescence (EL) images. Both [14] and [15] used the EL images of solar cells as the input dataset for a deep learning method to automatically detect and classify the defects of solar cells. In [16], the authors also built two detection models using a support vector machine (SVM) and CNN for an EL image dataset.

Furthermore, two other studies proposed different methods for detecting the defects of PV modules. In [17], an independent component analysis reconstruction algorithm was used to detect surface faults. Another novel algorithm was used in [18]. In this paper, local detection and global detection methods were proposed. In local detection, a water filling algorithm was used to determine the local maximum temperature of the PV panel region. Then, global detection, namely, multiframe recognition of PV faults, was adopted to further improve the anomalous detection accuracy of the local fault [18].

Pierdicca *et al.* proposed a CNN model to detect PV cell degradation using the VGG-16 network [19]. The authors used PV IR images to train the deep learning model, and an automatic recognition algorithm was then developed to detect PV module faults. Li *et al.* proposed a CNN solution for the defect detection of PV farms by using a drone to take IR pictures [20]. In [21], Nie *et al.* presented a CNN-based model to detect the hot spots of PV modules, and IR image data were used to train the CNN model. Grimaccia *et al.* also suggested a method with an image processing algorithm to detect defects using UAVs [22]. The PV modules could be classified into healthy, hot spots, bypass diodes, and disconnected. In [23], another method with an image processing algorithm was presented for the thermography defect detection of PV modules. These improved IR images could provide more details about the types of defects. In [24], an IR thermography system on a drone was developed to detect and locate malfunctioning PV modules. The K neighbors mean filter and Canny technique were used to preprocess these images.

However, based on a survey of previous works, we believe that the training image dataset could be further modified by the specifically designed image preprocessing technique, which should enhance the learning result with the emphasized contrast between normal cells and malfunctioning cells and then provide higher accuracy. Similarly, a numerical preprocessing method is proposed for the temperature dataset. Furthermore, we also select some particular statistical features to better train the machine learning model. Finally, a hybrid scheme embedded with these three detection procedures is proposed with even better accuracy. Many experiments are implemented to validate our proposals.

III. PROPOSED DETECTION SCHEME

In this section, we detail three proposed detection methods and one corresponding hybrid scheme that includes the deep learning algorithm, the image preprocessing method, the threshold function, and the machine learning algorithm. The parameter adjustment and feature selection steps are also introduced.

A. CNN DEEP LEARNING ALGORITHM

For the first two methods, the same CNN deep learning algorithm is chosen to train the detection models to assess whether a PV module has malfunctioned. Table 1 shows the CNN structure and feature extraction adopted in this study.

The architecture of the CNN consists of six convolutional layers, six max pooling layers and one fully connected layer. The convolutional layer is used to extract the features of the input data using kernels, and the output of the convolutional layer is a feature map. The objective of max pooling is to downsample an input image, and the output of the max pooling layer is the maximum value in each area. The fully

TABLE 1. CNN structure and feature extraction.

Layer	Shape	Parameters
Convolution	240, 320, 32	160
Max pooling	120, 160, 32	0
Convolution	120, 160, 64	8256
Max pooling	60, 80, 64	0
Convolution	60, 80, 128	32896
Max pooling	30, 40, 128	0
Convolution	30, 40, 256	131328
Max pooling	15, 20, 256	0
Convolution	15, 20, 512	524800
Max pooling	7, 10, 512	0
Convolution	7, 10, 1024	2098176
Max pooling	3, 5, 1024	0
Flatten	15360	0
Dense	256	3932416
Dense	2	514

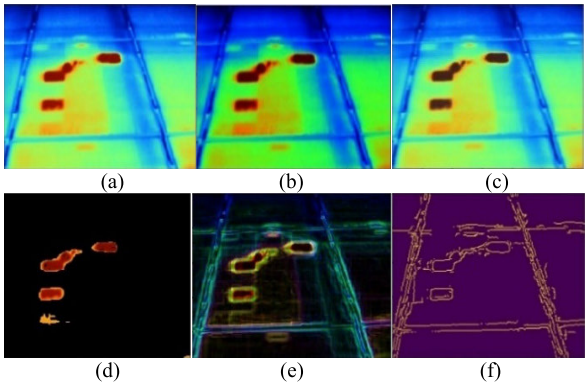

FIGURE 3. Illustration of image processing results. (a) No image processing, (b) Processed by gamma, (c) Processed by improved gamma, (d) Processed by the color mask, (e) Processed by Sobel and (f) Processed by Canny.

connected layer is used to flatten the output of the max pooling layer and then feed the results into neural networks.

B. IMPROVED GAMMA CORRECTION FUNCTION

In the first method, IR images are used to train the detection model. In general, an image preprocessing technique, the gamma correction function, can correct an image's luminance. However, to increase the detection efficiency, an improved gamma correction function is designed to enhance the contrast of the images of malfunctioning cells. In the gamma correction operation, an RGB (red, green and blue) image is converted into the HSV format first, where H represents the hue, S represents the saturation and V represents the value. In the improved gamma correction, we would like to make the red pixels more obvious than the other colors. Accordingly, the S and V values of red pixels are emphasized and adjusted by ρ thereafter. Fig. 3 (c) indicates that the red pixels become darker than the red pixels in Fig. 3 (a). In contrast to dark red pixels, the light red pixels do not become redder, as they are revised by the gamma correction in Fig. 3 (b). Creating a larger contrast for the red and light red pixels can cause larger differences between the defective locations and normal locations. The greater the difference, the easier the CNN model can distinguish between normal and abnormal PV modules during the detection process.

Algorithm 1 is the improved gamma correction function and includes the following four steps:

Improved gamma correction (image, gamma = 2)
Input PV module RGB-images (m × n)
Output PV module RGB-images (m × n)
for x = 1; x <= n **do**
  for y = 1; y <= m **do**
    convert image[x][y] (R,G,B) to image[x][y] (H,S,V)
  if (20,255,255) >= image[x][y] (H,S,V) >= (0,43,46) **then**
    S = S × ρ
    V = V × ρ
for x = 1; x <= n **do**
  for y = 1; y <= m **do**
    convert image[x][y] (H,S,V) to image[x][y] (R,G,B)
output = $(\frac{image}{255})^{gamma} \times 255$
return output

1) Convert the RGB image to the HSV format;
2) Multiply the S and V values of the pixels in the red range by ρ, i.e., $(20, 255, 255) \geq (H, S, V) \geq (0, 43, 46)$;
3) Convert the HSV image back to the RGB format;
4) Output the gamma correction with gamma = 2, as indicated in (3).

$$Output = (\frac{image}{255})^{gamma} \times 255 \tag{3}$$

Figs. 3 (a), (b) and (c) demonstrate the original image, the image processed by gamma correction and the image processed by improved gamma correction, respectively. Figs. 3 (d), (e) and (f) show the image processed by the color mask, the image processed by Sobel and the image processed by Canny, respectively. From these images, it is straightforward to conclude that Fig. 3 (c) presents a sharper contrast around the boundary.

C. THRESHOLD FUNCTION

In the second method, temperatures are used to train the learning model. Therefore, a threshold function is proposed to enhance the detection accuracy. This threshold function with two parts enlarges the numerical difference of the temperatures around the damaged area. The first part determines the value of threshold. The average temperature of all pixels in the image is calculated, and then the threshold value is chosen thereafter. If the average is larger than S, then the threshold is set as TU; otherwise, it is set as TL as described in (4), where $TU > TL$. The second part enlarges the contrast of the boundary of the damaged area. If temperature x is greater than

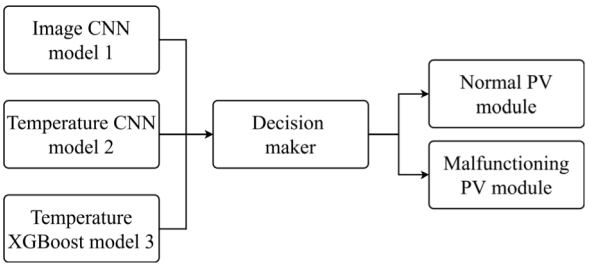

FIGURE 4. Flow chart of the hybrid scheme.

the average temperature plus the threshold, then return this temperature plus d; otherwise, return this temperature minus d, as shown in (5).

$$threshold = \begin{cases} TL, & mean \leq S \\ TU, & mean > S \end{cases} \tag{4}$$

$$f(x) = \begin{cases} x - d, & x < mean + threshold \\ x + d, & x \geq mean + threshold \end{cases} \tag{5}$$

D. XGBOOST AND THE HYBRID SCHEME

Since the abovementioned image and temperature CNN models learn and detect from the perspectives of colors and numbers, it is highly possible that they can complement each other. Moreover, to implement a hybrid detection-making scheme, we introduce the third machine learning algorithm called XGBoost for the temperature dataset. The XGBoost algorithm is designed to retrieve the statistical characteristics of the temperatures; nevertheless, the original CNN models are used to learn the general variation and distribution of temperatures. Thus, the major features of XGBoost will be chosen based on this criterion thereafter. Finally, the detection results of image CNN model 1, temperature CNN model 2 and temperature XGBoost model 3 are combined by using a decision maker. The final decision is made by the linear combination of these models. The flow chart of this hybrid detection scheme is described in Fig. 4.

E. PARAMETER ADJUSTMENT AND FEATURE SELECTION

As introduced earlier, the CNN models are trained to classify the malfunctioning modules and normal modules by using images and temperatures, respectively. Two preprocessing functions are designed to provide better performance. During two individual procedures that select better parameters, the key parameters of the improved gamma correction and threshold function are tuned according to the accuracy of the training result. The accuracies are chosen to be better than the 0.981 of the original gamma correction. Finally, two sets of parameters are decided. Fig. 5 shows the two respective adjustment processes using images with the improved gamma and temperature values with the threshold, and the detailed steps are described as follows.

1) A picture of a PV module was taken with an IR thermal imaging camera.
2) IR thermography was converted into image and temperature data.
3) Preprocess the image using an image processing technique, i.e., the improved gamma correction function, and preprocess the temperatures using the threshold function.
4) Input the image and temperature files into the CNN deep learning model individually.
5) Identify whether the PV module is malfunctioning or normal.
6) Adjust the parameters of the preprocessing functions and then repeat the above steps if the accuracy is less than 0.981.
7) Stop adjusting the parameters when the model is good enough (i.e., accuracy $>$ 0.981).

TABLE 2. XGBoost features.

	Features	Definition
1	max – min	Difference between the max and min temperatures in the file
2	max – median	Difference between the max and median temperatures in the file
3	30% std	Standard deviation of the first 30% of the temperatures in the file
4	1% ave – ave	Difference between the average of the first 1% and the average temperatures in the file
5	2% ave – 2%~10% ave	Difference between the average of the first 2% and the average of the first 2%~10% temperatures in the file

For the image dataset, we observe, test and conclude that the best ρ for the improved gamma correction function is 0.5 to emphasize red pixels within the range of $(20, 255, 255) \geq (H, S, V) \geq (0, 43, 46)$.

For the temperature dataset, if the temperature file has an average (i.e., mean) larger than 27 °C, the threshold should be equal to 2.5. Otherwise, it is 1, as indicated in (6). Then, all temperature values have 3 added to them if they are larger than or equal to the $mean + threshold$. Otherwise, all temperature values have 3 subtracted, as shown in (7). This is because we find that the best d is 3 for this dataset after repeated testing.

$$threshold = \begin{cases} 1, & mean \leq 27 \\ 2.5, & mean > 27 \end{cases} \tag{6}$$

$$f(x) = \begin{cases} x - 3, & x < mean + threshold \\ x + 3, & x \geq mean + threshold \end{cases} \tag{7}$$

The XGBoost algorithm is designed to learn the statistical characteristics of the temperature variations, and therefore, the following five major features, as listed in Table 2, are selected.

IV. EXPERIMENTAL RESULTS

In this section, we detail the dataset, experimental environment and results. The thermographic inspection data taken from a thermographic camera are converted into Comma

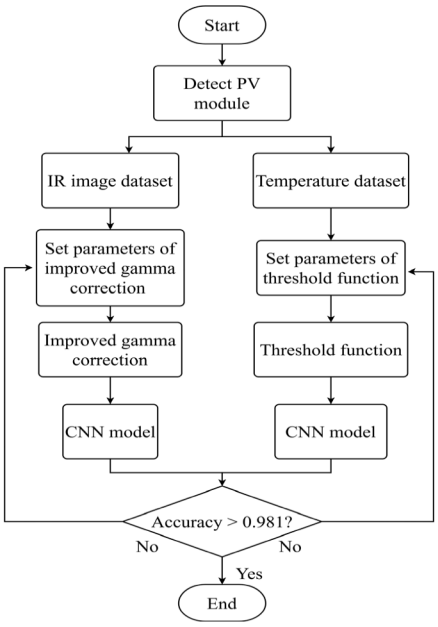

FIGURE 5. Two parameter adjustment flows using images with improved gamma and temperatures with a threshold function.

Separated Values (CSV) files of temperatures first. Both the image files and temperature files are adjusted by the correction function and threshold function, respectively. Then, these outputs and selected features are inputted into the CNN models and the XGBoost model for individual learning and identification.

A. EXPERIMENTAL DATASET

The thermal images are collected from the roof of the Industrial Technology Research Institute in Hsinchu, Taiwan. This thermographic inspection dataset includes 684 images and 684 converted temperature CSV files as follows.

1) These 240 × 320 thermographic images include 189 images for normal PV modules and 495 images for malfunctioning PV modules. Some samples are shown in Fig. 6.
2) These 240 × 320 CSV files include 189 CSV files for normal PV modules and 495 CSV files for malfunctioning PV modules.

Approximately 76% of the data are used as the training dataset, and approximately 24%, i.e., 161 photovoltaic modules, are used as the detection test set. To deal with the imbalanced data, we double train the minor classes of data during the training processes [25].

B. EXPERIMENTAL ENVIRONMENT

The hardware used for this experiment is a server equipped with an Nvidia GeForce RTX 2080 Ti GPU, an 8 core CPU and 64 GB of RAM. The software includes two parts. The first one, TensorFlow, is a deep learning framework and is an open source software library developed by Google that is widely used for machine learning and deep learning. The second is

TABLE 3. Confusion matrix.

	Actual	
Predicted	True negatives (TN) False negatives (FN)	False positives (FP) True positives (TP)

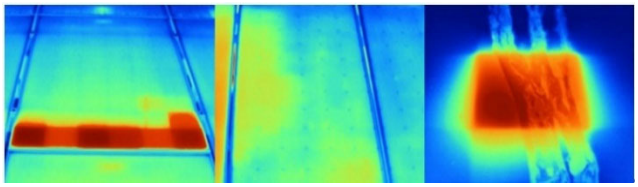

FIGURE 6. Thermographic images.

Keras, which is a high-level deep learning API written in Python. Keras allows users to build deep learning models with minimal code and time.

C. CLASSIFICATION ACCURACY

To evaluate the performance of the proposed methods, the following formula for the classification accuracy is employed and shown in (8). The formula is calculated based on the confusion matrix in Table 3.

$$Accuracy = \frac{TP + TN}{TP + TN + FP + FN} \tag{8}$$

D. CLASSIFICATION STEPS

After the thermal image dataset is generated from the thermographic camera, the images are converted to temperatures first. Then, either dataset is forwarded to the enhancement function as in step (1) and is further fed into the CNN model for classification as in step (2). In step (3), five major features are calculated using the temperatures and then inputted to the XGBoost model. Finally, the outputs of the above models are used to decide if a PV module is malfunctioning or normal, as in step (4).

1) Preprocess the IR thermographic images using the improved gamma correction function and preprocess the temperatures using the threshold function.
2) Forward the enhanced image file and the temperature file to the CNN deep learning models. In the second model, temperatures are used to complete the one-dimensional matrix.
3) Five major features were calculated and then fed into the XGBoost model.
4) Identify the PV module as malfunctioning or normal using the outputs of the above models.

E. DETECTION ACCURACY USING IMAGE AND TEMPERATURE CNNS

The performances of the proposed image CNN model with the improved gamma correction function and some other image processing methods are listed in Table 4. We also test many different kinds of image processing techniques to demonstrate the usefulness of the improved gamma. Each

TABLE 4. Comparison of some image processing techniques.

Image processing technique	Average accuracy
No image preprocessing	0.915
Sobel	0.882
Canny	0.826
Gamma correction	0.923
Color mask	0.857
Gamma + Sobel	0.876
Gamma + Canny	0.810
Gamma + Color mask	0.839
Improved gamma correction	0.938

TABLE 5. Confusion matrix for test with temperatures (240 × 320).

Model	Actual malfunctioning	Actual normal
Predicted malfunctioning	99	2
Predicted normal	1	59

technique is implemented three times, and then the average accuracy is calculated. As predicted, preprocessing of the improved gamma correction achieves the highest detection accuracy of 0.938.

The average detection accuracy of the proposed CNN model using the temperatures of PV modules with the threshold function is 0.946, and the best one is 0.981. Table 5 displays the confusion matrix for the best result.

This temperature CNN method also performs well with high accuracy. However, it takes a longer time to generate detection results, as does the detection model using the images with the improved gamma correction function. The inefficiency should be due to both of the mathematical operations, i.e., the improved gamma correction and the threshold function. Therefore, an image compression method is adopted to reduce the IR images from 240 × 320 to a size ranging from 240 × 160 to 60 × 80. We think that this method decreases the sizes of both the image and temperature datasets and should shorten the calculation times. Then, the accuracies and time consumptions of various compression ratios are experimented and summarized in Table 6. Each compression ratio is implemented three times, and the best accuracy is emphasized in bold. The average accuracies are calculated and listed in the next column. Comparing the first and second rows in the upper half and lower half of Table 6, respectively, it is easy to conclude that both improvement functions, i.e., improved gamma correction and the threshold enhance the accuracy of detection but consume more calculation time. Contrasting all rows except the first one in the upper half and lower half of Table 6, we indeed find that compression reduces the calculation times; however, overcompression is not good for detection accuracy. Figs. 7 and 8 illustrate the higher accuracy, lower accuracy and average accuracy with various compression ratios for the image and temperature detection methods, respectively.

120 × 160 is the best size for the image CNN detection model, and 80 × 160 is the best size for the temperature

TABLE 6. Comparison of various compression ratios.

Detection with various compression ratios	Accuracies for three tests	Average accuracy	Calculation time
Image detection w/o preprocessing/ 240×320	**0.925**/0.907/0.913	0.915	0.60959 s
Image detection with improved gamma/ 240×320	0.932/**0.957**/0.925	0.938	94.06232 s
Image detection with improved gamma/ 240×160	0.925/**0.950**/0.932	0.936	46.00155 s
Image detection with improved gamma/ 120×160	0.988/0.981/**1.000**	0.990	22.7584 s
Image detection with improved gamma/ 80×160	**0.969**/**0.969**/0.963	0.967	16.96005 s
Image detection with improved gamma/ 80×80	0.950/**0.957**/0.944	0.950	8.33431 s
Image detection with improved gamma/ 60×80	0.957/0.963/**0.969**	0.963	6.31298 s
Temperature detection w/o threshold/ 240×320	**0.894**/0.882/0.826	0.867	6.70284 s
Temperature detection with threshold/ 240×320	**0.981**/0.901/0.957	0.946	13.06552 s
Temperature detection with threshold/ 240×160	0.969/0.944/**0.981**	0.965	6.89181 s
Temperature detection with threshold/ 120×160	**0.988**/0.963/0.981	0.977	3.53061 s
Temperature detection with threshold/ 80×160	**0.988**/**0.988**/0.981	0.986	2.44495 s
Temperature detection with threshold/ 80×80	**0.981**/0.969/**0.981**	0.977	1.62259 s
Temperature detection with threshold/ 60×80	**0.988**/0.975/0.981	0.981	1.31719 s

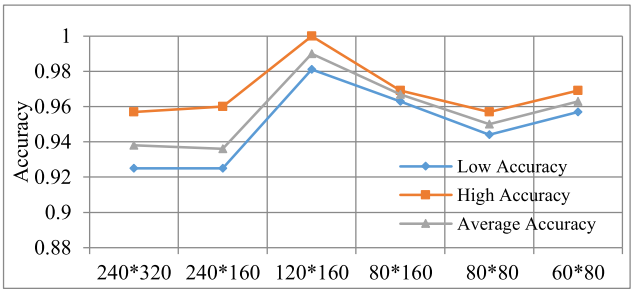

FIGURE 7. Comparison of various compression ratios for image CNN model.

CNN detection model. These two rows are thus highlighted in shade in Table 6. We believe that larger datasets or smaller datasets may cause the learning methods to limit focus on irregularity or to focus too much on irregularity. Therefore, medium compression ratios are more appropriate for both CNN models.

F. HYBRID DETECTION SCHEME WITH THREE MODELS

In addition to two CNN models, the third one we chose is the XGBoost algorithm. The reason why we select XGBoost is that it performs better than many other machine learning algorithms for our experimental dataset, as indicated in Table 7.

To optimize the accuracy of the proposed hybrid detection scheme, we use the combination of the best compression

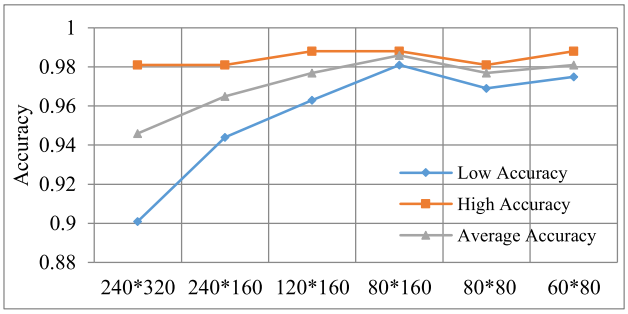

FIGURE 8. Comparison of various compression ratios for temperature CNN model.

TABLE 7. Comparison of some machine learning techniques.

Machine learning techniques	Average accuracy
XGBoost	0.950
Gradient boosting	0.938
Decision tree	0.845
SVM	0.938

ratios of the image and temperature CNN models, i.e., 120 × 160 for the image CNN algorithm and 80 × 160 for the temperature CNN algorithm with the XGBoost model. They are of equal weights in the decision-making procedure. The detailed procedure of the hybrid scheme is illustrated in Fig. 9. From the IR camera, the image and temperature datasets are created. The images are compressed to 120 × 160 first and preprocessed by the improved gamma correction function. Then, they are forwarded to Image CNN model 1 for detection. The temperatures are compressed to 80 × 160 and preprocessed by a threshold function. These numbers are passed to Temperature CNN model 2 for judgment. The specific features of the temperatures are also retrieved and then sent to Temperature XGBoost model 3 for third detection. The outcomes of these models are aggregated by the decision maker to generate the final detection result.

A total of nine tests are implemented, and the average accuracy is 0.992. Six of these nine results have an accuracy of 0.994, and three have an accuracy of 0.987. As predicted earlier, the complementary design works somewhat well. To clarify that the proposed methods are effective, we also compare our method with other approaches, and the details are shown in Table 8. As observed, our methods are ranked in the top tier. The CNN is the major efficient deep learning method used for detecting the defects of PV modules. However, both of our CNN proposals outperform the other CNN schemes proposed in [13], [16], [19], [21] and achieve very close performance to the first-tier methods presented in [14], [20]. In fact, [14] used an EL image dataset to implement detection, but EL images were typically collected in a dark environment to reduce background light [26]. This may not be good for the operation of UAVs. Reference [20] adopted a visible image dataset; nevertheless, visible images were tremendously affected by the lightness of the sky, which may vary the accuracy of detection. Finally, the proposed hybrid scheme functions better than any single method as expected.

TABLE 8. Comparison on different methods.

Learning methods	Dataset(s)	Preprocessing	Accuracy
CNN [13]	2-D scalograms	No	0.735
CNN [14]	EL image	No	0.993
CNN [16]	EL image	Masking	0.884
Water filling [18]	Visible image	No	0.903
VGG16 (CNN) [19]	IR image	No	0.937
CNN [20]	Visible image	No	0.978~0.995
CNN [21]	IR image	No	0.95
Proposed image CNN	IR image /120×160	Improved gamma	0.990
Proposed temperature CNN	Temperatures /80×160	Threshold function	0.986
Proposed hybrid scheme (CNNs & XGBoost)	Hybrid (IR image and temperatures)	Improved gamma & threshold functions	0.992

TABLE 9. Number of modules after using data augmentation.

	Original set of modules	Extended set of faulty modules	Used for detection test within extended set
Hot spot	424	424	105
PID	64	384	95
Open circuit	7	44	10
Normal	189		

TABLE 10. Confusion matrix of testing.

	Actual hot spot	Actual PID	Actual open circuit
Predicted hot spot	100	7	1
Predicted PID	4	88	0
Predicted open circuit	1	0	9

G. FURTHER CLASSIFICATION OF THE DEFECTS OF PHOTOVOLTAIC MODULES

Since different PV module defects may require different maintenance procedures, this study also tries to further classify the defect types. As introduced earlier, the major defect types include hot spots, PIDs and open circuits. However, the numbers of PID and open circuit modules are insufficient. To train a detection model, we generate more PID and open circuit data using a data augmentation method [27], as shown in Table 9. To achieve better accuracy, we select the image CNN model with 120 × 160 images. The performance of our classification model is 0.938, and Table 10 demonstrates the confusion matrix of the classification results. From this table, it is observed that the classification of actual PID and open circuit defects is not that good compared to hot spot defects. Therefore, if the classification is critical for some maintenance programs, then a preprocessing algorithm to stress the characteristics of PID and open circuit defects may be necessary for even better accuracy of classification models.

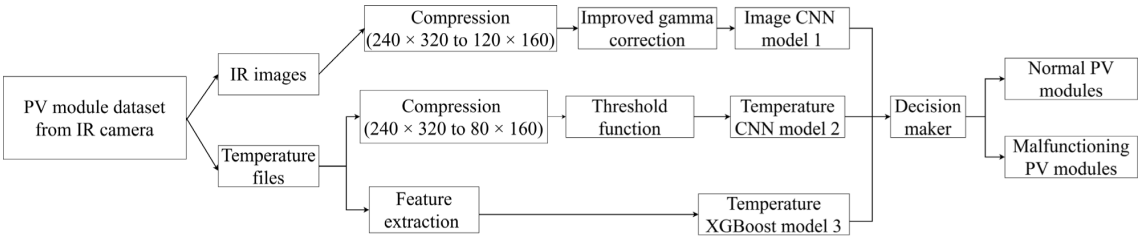

FIGURE 9. Detailed procedure of the hybrid detection scheme.

V. CONCLUSION

We have proposed a hybrid detection scheme with three embedded learning methods that can be used to detect malfunctioning PV modules with high accuracy. For the first method, the CNN model is trained using IR images, which are preprocessed by the improved gamma correction to emphasize the high temperatures with deeper reds. We test different image processing techniques that are expected to highlight the color of malfunctioning ones, and the improved gamma correction we design is the most suitable algorithm for our purpose. For the second method, the CNN model is trained using the temperature dataset, which is preprocessed using a threshold function, and it can accurately detect malfunctioning modules as well. To enhance the contrast of the malfunctioning modules, a threshold function is designed to process the temperature files in advance. However, the improved gamma correction and the threshold function consume considerable processing time. To solve the time-consumption issue for the extra preprocesses, we adopt a compression method. That is, the sizes of the IR images and corresponding temperature files are reduced from 240×320 to some smaller ones ranging from 60×80 to 240×160. Therefore, the time consumption is tremendously decreased by reducing the mathematical calculations. In addition, we retrieve the specific statistical features regarding the variation in temperatures to train the third XGBoost algorithm. This hybrid detection scheme achieves very good detection accuracy for our dataset. Because the major phenomenon of malfunctioning PV modules is unusual high temperatures, all of our designs focus on identifying them. Consequently, we believe that the good detection accuracy of our hybrid scheme can be validated for the other datasets as well.

To also classify the kinds of PV defects, we train a CNN model using 120×160 IR images that are preprocessed using the improved gamma function. This CNN model also achieves a decent performance. As explained earlier, we think that a UAV equipped with an IR camera is a good carrier to take IR pictures. After these pictures have been retrieved, the corresponding images and temperatures and the proposed detection methods can be used to construct an efficient maintenance program for medium- to large-scale solar power plants.

REFERENCES

[1] R. Ebner, B. Kubicek, and G. Ujvari, "Non-destructive techniques for quality control of PV modules: Infrared thermography, electro-and photoluminescence imaging," in *Proc. 39th Annu. Conf. IEEE Ind. Electron. Soc. (IECON)*, Nov. 2013, pp. 8104–8109, doi: 10.1109/iecon.2013.6700488.

[2] C. Buerhop, D. Schlegel, M. Niess, C. Vodermayer, R. Weißmann, and C. J. Brabec, "Reliability of IR-imaging of PV-plants under operating conditions," *Sol. Energy Mater. Sol. Cells*, vol. 107, pp. 154–164, Dec. 2012, doi: 10.1016/j.solmat.2012.07.011.

[3] A. Krizhevsky, I. Sutskever, and G. E. Hinton, "ImageNet classification with deep convolutional neural networks," *Commun. ACM*, vol. 60, no. 6, pp. 84–90, May 2017, doi: 10.1145/3065386.

[4] Q. Li, W. Cai, X. Wang, Y. Zhou, D. D. Feng, and M. Chen, "Medical image classification with convolutional neural network," in *Proc. 13th Int. Conf. Control Automat. Robot. Vis. (ICARCV)*, Dec. 2014, pp. 844–848, doi: 10.1109/icarcv.2014.7064414.

[5] T. Chen and C. Guestrin, "XGBoost," in *Proc. 22nd ACM SIGKDD Int. Conf. Knowl. Discovery Data Mining*, Aug. 2016, pp. 1–4, doi: 10.1145/2939672.2939785.

[6] D. Nielsen, "Tree boosting with XGBoost: Why does XGBoost win every machine learning competition," M.S. thesis, Dept. Phys. Math., Norwegian Univ. Sci. Technol., Trondheim, Norway, Dec. 2016. [Online]. Available: https://ntnuopen.ntnu.no/ntnu-xmlui/bitstream/handle/11250/2433761/16128_FULLTEXT.pdf?sequence=1&isAllowed=y

[7] D. Zhang, L. Qian, B. Mao, C. Huang, B. Huang, and Y. Si, "A data-driven design for fault detection of wind turbines using random forests and XGboost," *IEEE Access*, vol. 6, pp. 21020–21031, 2018, doi: 10.1109/access.2018.2818678.

[8] Z. Chen, F. Jiang, Y. Cheng, X. Gu, W. Liu, and J. Peng, "XGBoost classifier for DDoS attack detection and analysis in SDN-based cloud," in *Proc. IEEE Int. Conf. Big Data Smart Comput. (BigComp)*, Jan. 2018, pp. 251–256, doi: 10.1109/bigcomp.2018.00044.

[9] C. Poynton, *Digital Video and HD: Algorithms and Interfaces*, 2nd ed. Amsterdam, The Netherlands: Elsevier, 2012.

[10] M. Aghaei, A. Gandelli, F. Grimaccia, S. Leva, and R. E. Zich, "IR real-time analyses for PV system monitoring by digital image processing techniques," in *Proc. Int. Conf. Event-Based Control, Commun., Signal Process. (EBCCSP)*, Jun. 2015, pp. 1–6, doi: 10.1109/ebccsp.2015.7300708.

[11] J. A. Tsanakas, D. Chrysostomou, P. N. Botsaris, and A. Gasteratos, "Fault diagnosis of photovoltaic modules through image processing and canny edge detection on field thermographic measurements," *Int. J. Sustain. Energy*, vol. 34, no. 6, pp. 351–372, Jul. 2015, doi: 10.1080/14786451.2013.826223.

[12] A. Chouder and S. Silvestre, "Automatic supervision and fault detection of PV systems based on power losses analysis," *Energy Convers. Manage.*, vol. 51, no. 10, pp. 1929–1937, Oct. 2010, doi: 10.1016/j.enconman.2010.02.025.

[13] F. Aziz, A. Ul Haq, S. Ahmad, Y. Mahmoud, M. Jalal, and U. Ali, "A novel convolutional neural network-based approach for fault classification in photovoltaic arrays," *IEEE Access*, vol. 8, pp. 41889–41904, 2020, doi: 10.1109/access.2020.2977116.

[14] M. R. U. Rahman and H. Chen, "Defects inspection in polycrystalline solar cells electroluminescence images using deep learning," *IEEE Access*, vol. 8, pp. 40547–40558, 2020, doi: 10.1109/access.2020.2976843.

[15] A. Bartler, L. Mauch, B. Yang, M. Reuter, and L. Stoicescu, "Automated detection of solar cell defects with deep learning," in *Proc. 26th Eur. Signal Process. Conf. (EUSIPCO)*, Sep. 2018, pp. 2035–2039, doi: 10.23919/eusipco.2018.8553025.

[16] S. Deitsch, V. Christlein, S. Berger, C. Buerhop-Lutz, A. Maier, F. Gallwitz, and C. Riess, "Automatic classification of defective photovoltaic module cells in electroluminescence images," *Sol. Energy*, vol. 185, pp. 455–468, Jun. 2019, doi: 10.1016/j.solener.2019.02.067.

[17] X. Zhang, H. Sun, Y. Zhou, J. Xi, and M. Li, "A novel method for surface defect detection of photovoltaic module based on independent component analysis," *Math. Problems Eng.*, vol. 2013, Sep. 2013, Art. no. 520568, doi: 10.1155/2013/520568.

[18] V. Carletti, A. Greco, A. Saggese, and M. Vento, "An intelligent flying system for automatic detection of faults in photovoltaic plants," *J. Ambient Intell. Hum. Comput.*, vol. 11, no. 5, pp. 2027–2040, May 2020, doi: 10.1007/s12652-019-01212-6.

[19] R. Pierdicca, E. S. Malinverni, F. Piccinini, M. Paolanti, A. Felicetti, and P. Zingaretti, "Deep convolutional neural network for automatic detection of damaged photovoltaic cells," *Int. Arch. Photogramm., Remote Sens. Spatial Inf. Sci.*, vol. 42, pp. 893–900, May 2018, doi: 10.5194/isprs-archives-xlii-2-893-2018.

[20] X. Li, Q. Yang, Z. Lou, and W. Yan, "Deep learning based module defect analysis for large-scale photovoltaic farms," *IEEE Trans. Energy Convers.*, vol. 34, no. 1, pp. 520–529, Mar. 2019, doi: 10.1109/tec.2018.2873358.

[21] J. Nie, T. Luo, and H. Li, "Automatic hotspots detection based on UAV infrared images for large-scale PV plant," *Electron. Lett.*, vol. 56, no. 19, pp. 993–995, Sep. 2020, doi: 10.1049/el.2020.1542.

[22] F. Grimaccia, S. Leva, and A. Niccolai, "PV plant digital mapping for modules' defects detection by unmanned aerial vehicles," *IET Renew. Power Gener.*, vol. 11, no. 10, pp. 1221–1228, Aug. 2017, doi: 10.1049/iet-rpg.2016.1041.

[23] M. W. Akram, G. Li, Y. Jin, X. Chen, C. Zhu, X. Zhao, M. Aleem, and A. Ahmad, "Improved outdoor thermography and processing of infrared images for defect detection in PV modules," *Sol. Energy*, vol. 190, pp. 549–560, Sep. 2019, doi: 10.1016/j.solener.2019.08.061.

[24] P. Zhang, L. Zhang, T. Wu, H. Zhang, and X. Sun, "Detection and location of fouling on photovoltaic panels using a drone-mounted infrared thermography system," *J. Appl. Remote Sens.*, vol. 11, no. 1, Feb. 2017, Art. no. 016026, doi: 10.1117/1.jrs.11.016026.

[25] M. Buda, A. Maki, and M. A. Mazurowski, "A systematic study of the class imbalance problem in convolutional neural networks," *Neural Netw.*, vol. 106, pp. 249–259, Oct. 2018, doi: 10.1016/j.neunet.2018.07.011.

[26] S. Johnston, "Contactless electroluminescence imaging for cell and module characterization," in *Proc. IEEE 42nd Photovolt. Spec. Conf. (PVSC)*, New Orleans, LA, USA, Jun. 2015, pp. 1–6, doi: 10.1109/PVSC.2015.7356423.

[27] C. Shorten and T. M. Khoshgoftaar, "A survey on image data augmentation for deep learning," *J. Big Data*, vol. 6, no. 1, Dec. 2019, Art. no. 60, doi: 10.1186/s40537-019-0197-0.

HUMBLE PO-CHING HWANG received the B.S. degree from the Department of Business Administration, National Chung Cheng University, Chiayi, Taiwan, in 2017. He is currently pursuing the Ph.D. degree with the Institute of Information Management, National Yang Ming Chiao Tung University, Hsinchu, Taiwan. His research interests include machine and deep learning, solar energy, information security, and game theory.

COOPER CHENG-YUAN KU (Member, IEEE) received the B.S. degree in control engineering from National Chiao Tung University, Taiwan, in 1987, and the M.S. and Ph.D. degrees in electrical engineering from Northwestern University, USA, in 1993 and 1995, respectively. From 1999 to 2014, he was with the Department of Information Management, National Chung Cheng University. Since 2014, he has been with the Institute of Information Management, National Yang Ming Chiao Tung University, Hsinchu, Taiwan. His current research interests include artificial intelligence, information security and management, blockchain systems, the Internet of Things, and data communication networks.

JAMES CHI-CHANG CHAN was born in Taipei, Taiwan, in January1958. He received the Ph.D. degree from the Computer-Aided Engineering (CAE) Group, Department of Civil Engineering, National Taiwan University. Since 1989, he has been with the Laboratory of Research and Development, Industrial Technology Research Institute (ITRI). His research interests include computer-aided engineering, engineering information technology, structure safety non-destructive detection, civil and disaster prevention, solar PV system planning and evaluation design, solar PV system detection and evaluation, solar PV system data value-added analysis, and solar BIPV systems.